Journal of Materials Chemistry C

Quantifying Polaron Densities in Sequentially Doped Conjugated Polymers: Exploring the Upper Limits of Molecular Doping and Conductivity

Journal:	*Journal of Materials Chemistry C*
Manuscript ID	TC-ART-05-2023-001569.R2
Article Type:	Paper
Date Submitted by the Author:	03-Oct-2023
Complete List of Authors:	Murrey, Tucker; University of California Davis Department of Chemical Engineering and Materials Science, Materials Science Engineering Berteau-Rainville, Melissa; Institut national de la recherche scientifique Centre energie Materiaux Telecommunications Gonel, Goktug; UC Davis, Chemical Engineering Saska, Jan; UC Davis, Chemistry Shevchenko, Nikolay; UC Davis, Chemistry Fergerson, Alice; University of California Davis; Princeton University Talbot, Rachel; UC Davis, Chemical Engineering Yacoub, Nichole; University of California Davis Zhang, Fengyu; Princeton University Kahn, Antoine; Princeton University, Department of Electrical Engineering Mascal, Mark; UC Davis, Chemistry Salzmann, Ingo; Concordia University, Physics, Chemistry Moule, Adam; UC Davis, Chemical Engineering and Materials Science

Quantifying Polaron Densities in Sequentially Doped Conjugated Polymers: Exploring the Upper Limits of Molecular Doping and Conductivity

Tucker L. Murrey,[*,†,‡] Melissa Berteau-Rainville,[¶] Goktug Gonel,[§] Jan Saska,[‖] Nikolay E. Shevchenko,[‖] Alice S. Fergerson,[§,#] Rachel M. Talbot,[§] Nichole L. Yacoub,[§] Fengyu Zhang,[‡] Antoine Kahn,[‡] Mark Mascal,[‖] Ingo Salzmann,[⊥] and Adam J. Moulé[*,§]

†*Department of Material Science and Engineering, University of California, Davis, CA, USA*

‡*Department of Electrical and Computer Engineering, Princeton University, Princeton, NJ, USA*

¶*Institut National de la Recherche Scientifique (INRS), Centre Energie Materiaux Telecommunications, Varennes, QC, Canada*

§*Department of Chemical Engineering, University of California, Davis, CA, USA*

‖*Department of Chemistry, University of California, Davis, CA, USA*

⊥*Department of Physics, Department of Chemistry & Biochemistry, Concordia University, Montréal, QC, Canada*

#*Current address: Department of Chemical and Biological Engineering, Princeton University, Princeton, NJ, USA*

E-mail: tlmurrey@ucdavis.edu; amoule@ucdavis.edu

Phone: +1 (530) 754-8669

Introduction

Fine control over the charge carrier density is essential for optimizing the functions of nearly all modern electronic devices. Carrier densities in inorganic semiconductors are typically controlled by introducing elements of different valency via atomic substitution within the crystal lattice of the semiconductor to achieve p-/n-type doping, respectively.[1,2] The prototypical inorganic semiconductor, silicon, becomes degenerately doped above a dopant concentration of $\sim 10^{18}$ molecules $\cdot$ cm^{-3}, where it turns essentially metallic.[3] Below this limit, the mobile hole/electron density is equal to the p-/n dopant density. Since substitutional doping is incompatible with semiconducting polymers (SPs) much attention has been given to molecular doping as a method for controlling carrier density, where molecular acceptors/donors are intermixed with the polymer host.[4–6] The development of sequential solution p-type doping strategies has led to impressive conductivities in thin films in the range of 100 – 1000 S cm^{-1} for many polymers because, in contrast to doping from a mixed polymer/dopant solution blend, the microstructure, and therefore the charge carrier mobility, remains largely unperturbed.[7–14] However, this approach intrinsically lacks quantification of the active dopant loading, an issue that we aim to address in the present article by introducing a model to quantify the dopant induced carrier density in sequentially p-type doped polymer films.

Various research groups have shown that within a sequentially doped polymer film, there can exist a mixture of neutral polymer sites, singly charged (polaronic) sites, and doubly charged (bipolaronic) sites in a ratio dependent on the strength, concentration, and the valence state of the dopant.[15–20] The assignment of these different species is typically based directly on ultraviolet-visible- near infrared absorption (UV-vis-NIR) measurements where spectral features characteristic for the respective charged states are observed. In principle, the ratio between neutral:polaron:bipolaron sites could also be quantified in this way.[21,22] A major practical challenge for calculating charge density in sequentially doped polymer films is that the number of polymer sites per volume that are effectively "dopable" is unknown. This uncertainty arises because the average polaron delocalization length in conjugated poly-

mers remains speculative and may differ within the same polymer depending on the anion size, location, and doping density.[23] In an undoped (low dielectric constant) film, polarons induced by field effect delocalize over many monomers.[18] In doped films, however, the polaron is strongly localized by Coulombic attraction to the dopant counterion.[17] Additionally, the uncertainty in polaron density is greater in sequentially doped films compared to premixed dopant/polymer solutions because the film dopant density is not determined by the mixing ratio, but rather, it is controlled by a multi-component equilibrium.[24] Finally, not all molecular dopants induce a charge separated polaron state, but instead may produce a bound charge transfer state or the dopant may not ionize but remains neutral making the ratio of neutral to charged dopants difficult to determine.[5] While several groups have presented methods for calculating the charge distributions between polymers and molecular dopants, direct experimental evidence is limited.[5,8,25,26] Typically, in such studies only a single polymer is probed, either doped with a single molecular dopant, or comparing several dopants. Overall, this long list of factors, together with the fact that different methods are employed by different research groups, leads to huge variations in the reported charge densities. Certain techniques, such as Hall effect measurements, are prone to systematic uncertainty when probing organic semiconductors and tend to overestimate the total carrier density and therefore underestimate mobility.[27]

Accurate quantification of charge density is highly desirable and is the main subject of this article. Semiconductor band models that are used to characterize electronic devices require an accurate and reliable determination of the charge carrier density. Any comparison between different semiconductors requires some knowledge of the doping level and charge carrier density. We present here a simple method, based on optical measurements, to model and quantify the carrier density in molecularly doped conjugated polymer films. We validate this method by comparison with density of states (DOS) simulations as a function of the dopant density that show near quantitative agreement among eleven polymer/dopant combinations. The methodology presented yields a self-consistent quantitative comparison

of polaron density between several polymers and dopants with different IE's and EA's, respectively.

Results and Discussion

Optical Carrier Density Model

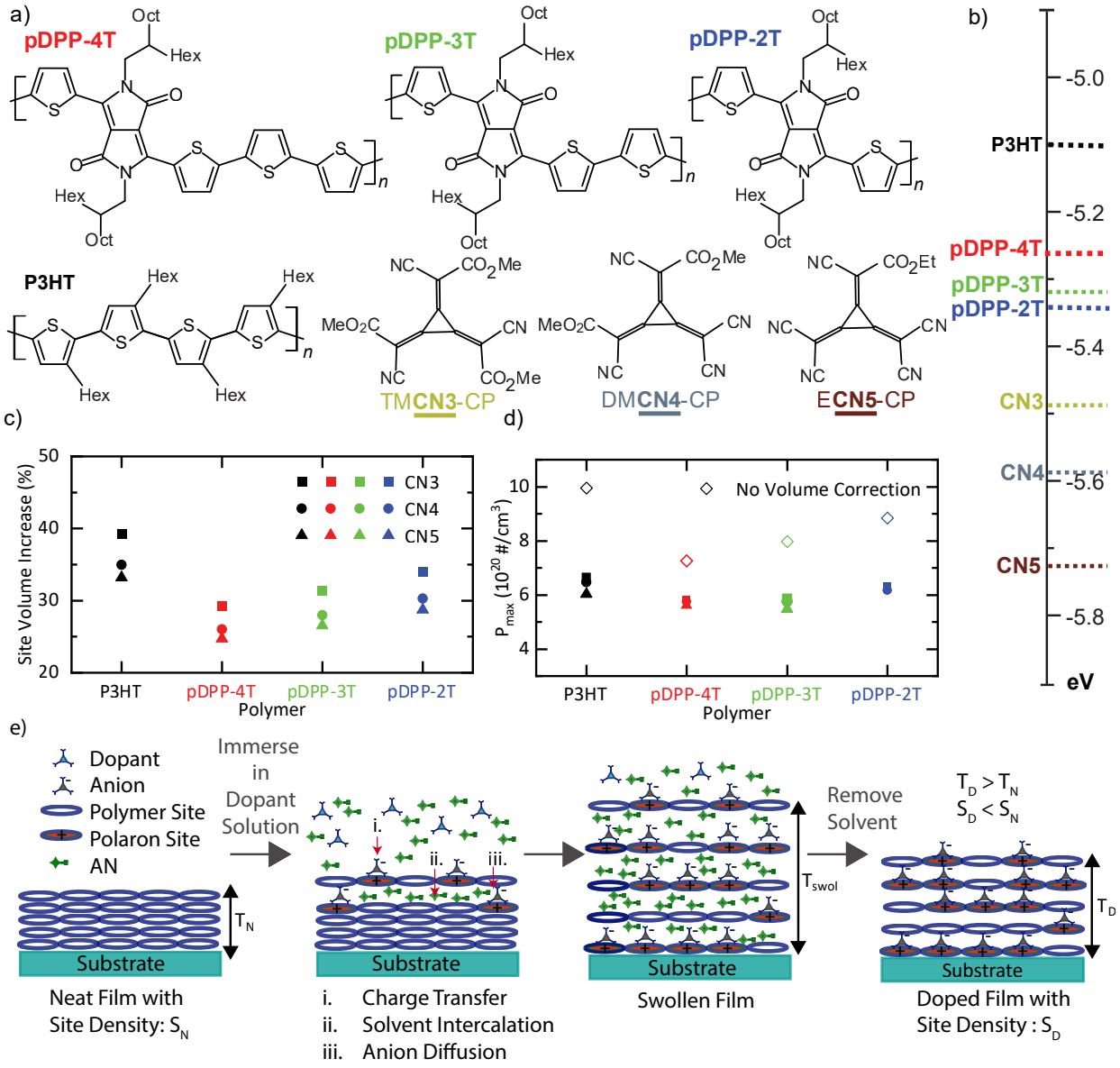

Figure 1: **Material Properties:** a) Molecular structures of the polymer "sites" and dopants. b) Ionization Energies (IE) of the polymers and the electron affinities (EA) of the dopants obtained using cyclic voltometry (CV) and plotted with respect to the vacuum level. c) Increase in site volumes with the addition of an interstitial dopant. d) Maximum theoretical polaronic charge density with (closed symbols) and without (open symbols) correcting for the film thickness expansion caused by addition of molecular dopants. e) Illustration of the sequential solution doping process including solvent swelling and film expansion during sequential doping followed by film collapse during solvent evaporation.

In this section, we introduce the molecular formulas of the polymers and dopants. We define a polymer "site" volume and show how this site volume must necessarily increase as dopant anions are added to the film. We reintroduce our optical method to calculate the polaron mole fraction (Θ) from optical measurements. Using relatively simple mass balance calculations these site volumes enable a reliable calculation of the polaron density as a function of Θ and the relative ratio of the polymer "site" to anion "site" ratio. We also discuss methods to reliably compare the electrochemical doping level for pure samples of the polymers and dopants.

Structural formulas for the cyclopropane-based dopants; trimethyl 2,2',2"-(cyclopropane-1,2,3-triylidene)tris(cyanoacetate) (TMCN3-CP), dimethyl 2,2'-(3-(dicyanomethylene) cyclopropane -1,2-diylidene)bis(2-cyanoacetate) (DMCN4-CP), and ethyl [bis(dicyanomethylidene) cyclopropylidene] cyanoacetate (ECN5-CP); and the polymer "sites"; defined as the minimum delocalization length of a polaron along the polymer backbone, are displayed in Figure 1a. The studied polymers include the regioregular homopolymer, poly-3-hexylthiophene (P3HT), and a series of donor acceptor (D-A) copolymers composed of a diketopyrrolopyrrole (DPP) donor and either a 2-thiophene (2T), 3-thiophene (3T), or 4-thiophene (4T) acceptor groups. For the remainder of the article the molecular dopants, TMCN3-CP, DMCN4-CP, and ECN5-CP, will be referred to as CN3, CN4, and CN5, respectively, and the three D-A polymers will be referred to as pDPP-2T, pDPP-3T, and pDPP-4T. As previously reported,[28] the minimum polaron delocalization length for D-A co-polymers can be modeled with a single D-A polymer segment.[29] The "site" size for the homopolymer P3HT is more difficult to define, as the polaron delocalization length is highly dependent on the local dihedral disorder of the polymer backbone, which means that the delocalization length may change with polaron density.[30] This is reported to be in the range of 3 to 6 thiophene units in molecularly doped films.[17,23,31–33] For the purpose of this study, we assume a constant "site" size of 4 thiophene units in the P3HT films as shown by Untilova et. al.[34] Figure 1b depicts the ionization energy (IE) of the highest occupied molecular orbital (HOMO) of the

four polymers (5.10, 5.26, 5.31, and 5.33 eV for P3HT, pDPP-4T, pDPP-3T, and pDPP-2T, respectively) and the electron affinity (EA) of the lowest unoccupied molecular orbital (LUMO) of the three dopants (5.50, 5.61, and 5.75 eV for CN3, CN4, and CN5, respectively), as measured by CV referenced to Ag/AgCl.[28,35,36] The energy offset between the polymer HOMO and dopant LUMO energy levels provides an approximation of the energetic driving force for charge transfer ($\Delta E = EA - IE$) at low doping levels. At high doping levels the situation is more complex because the Fermi energy lies within the intrinsic polymer band and the relative energy difference between the polaron and dopant anion must be calculated using a DOS model. A greater $|\Delta E|$ typically results in larger polaron mole fractions at a given dopant solution concentration.[28] However, ΔE alone is not enough to quantify the full extent of the doping efficacy. There are a number of critical variables that affect the doping density in a sequentially doped polymer film including:

1. the porosity and crystallinity[26] of the host film,
2. the free energies of mixing between the polymer, processing solvent, and the molecular dopants,
3. the dielectric constant of the processing solvent,
4. entropic effects from structural rearrangements, and
5. the width of the DOS for the frontier orbital of the polymer.

Another commonly overlooked factor for accurate quantification of charge density in molecularly doped polymers is the need to account for the volume of the dopant. Unlike inorganic semiconductors, where dopants are typically substitutional, molecular dopants have significant volume and occupy interstitial locations between polymer chains.[37,38] We previously used neutron reflectometry (NR) to demonstrate that P3HT films sequentially doped to moderate doping levels ($\sim$2% by mass) with 2,3,5,6-tetrafluoro-7,7,8,8-tetracyanoquinodimethane (F4TCNQ) undergo a 10% increase in their thickness compared to the pristine films.[39] While

film thickness measurements may be used as a proxy for volume expansion, unfortunately NR experiments were not planned into this study. Future work is needed to directly probe film expansion as a function of the polaron fraction. As a simple approximation, the volume increase from the addition of molecular dopants can be modeled using Van der Waals (VdW) volumes (which is the volume derived from molecular mechanics software ChemAxon MarvinSketch version 19.21.5.).[40] The volume of a doped "site" (V_{DS}) on a polymer is equal to the sum of the native polymer site and dopant VdW volumes V_S and V_D, respectively. Figure 1c illustrates that the VdW volume of the P3HT, pDPP-4T, pDPP-3T, and pDPP-2T sites increases by 25–40% upon doping with CN3, CN4, and CN5. The VdW volumes are located in the Supporting Information. We have previously published a non-interacting site model that utilizes optical UV-vis-NIR absorption data to approximate the fraction of polymer sites that are occupied by a polaron in a sequentially doped film, i.e. the polaron mole fraction (Θ).[28] Assuming that 100% of the dopants remaining in the film are ionized, the average site volume (V_{Ave}) can be calculated using V_S, V_{DS}, and Θ.

$$V_{Ave}(\Theta) = V_S + \Theta V_D = (1 - \Theta) \cdot V_S + \Theta \cdot V_{DS} \quad (1)$$

We note that near complete dopant ionization is a reasonable assumption for these samples, as we previously reported that the neutral CN3, CN4, and CN5 absorption bands are not detected in any of the UV-vis-NIR spectra for the doped film.[28] We clarify that this optical method limits our detection of neutral dopants to a $\leq 5\%$ neutral to ionized dopant ratio.[28] Therefore, to simplify the model we assume that every dopant molecule remaining in the film yields one polaron on an ionized polymer site. In a case where there is a significant population of non-ionized dopant, Equation 1 underestimates the volume expansion, as it does not take into account the volume of non-ionized dopants within the film.

We now take this optical analysis one step further to obtain an approximation of carrier density. Figure 1d connects the polaron mole fraction obtained in the non-interacting site model to a quantifiable carrier density. This approximation begins with calculating the

site density in an undoped polymer ($S_N = \frac{\rho \cdot N_A}{M_s}$), using the polymer mass density (ρ = ~1.1 mg/mL), Avogadro's number (N_A), and the site mass (M_S). The absolute maximum polaronic carrier density is simply equal to S_N. In doped samples, the volume of the dopant must be accounted for as discussed below and further elaborated upon in the Supporting Information. Table 1 lists the intrinsic site densities for each polymer depicted in Figure 1a as well as two other commonly studied polymers. The intrinsic site density for P3HT as a function of the site size from 1 to 10 thiophene rings is depicted in Supporting Information Figure S4.

Table 1: Upper limits of polaronic and bipolaronic density calculated using the monomer density of the undoped polymer assuming no volume change upon doping; asterisked polymers commonly appear in literature and are displayed for comparison, but are not studied here. The site mass and density for P3HT is calculated for a site composed of four thiophene monomers.

Polymer	**Polaronic Maximum**	**Bipolaronic Maximum**
IDTBT*	5.1×10^{20} cm^{-3}	1.2×10^{21} cm^{-3}
pDPP-4T	7.3×10^{20} cm^{-3}	1.5×10^{21} cm^{-3}
pDPP-3T	7.8×10^{20} cm^{-3}	1.6×10^{21} cm^{-3}
pDPP-2T	8.8×10^{20} cm^{-3}	1.8×10^{21} cm^{-3}
P3HT	9.4×10^{20} cm^{-3}	1.9×10^{21} cm^{-3}
PBTTT*	1.0×10^{21} cm^{-3}	2.0×10^{21} cm^{-3}

Knowledge of the doping mechanism (i.e., polaron versus bipolaron formation), the neat site density S_N, the polaron mole fraction Θ, the intrinsic site volume, and the average site volume with respect to Θ, then enables a linear approximation of the carrier density. As previously reported,[28] CN3, CN4, and CN5 dopants undergo integer charge transfer with all four of the studied polymers forming positive polarons as mobile charge carriers, with no clear spectral indication of bipolarons being formed. Assuming that each site can either be unoccupied or occupied by a polaron, the carrier density ($P(\Theta)$) can be approximated using Equation 2:

$$P(\Theta) = S_N \cdot \Theta \cdot \frac{V_S}{V_{Ave}(\Theta)} \tag{2}$$

This simplified approach doesn't consider bipolaron occupancy on the polymers. As we previously reported,[28] the integrated area of near IR polaron P1 absorption peak (also in Figure S1) increases faster than the sum of the neutral absorbance integrals decrease (for P3HT only), potentially indicating the presence of polaron-polaron interactions, which might be an indication of bipolaron formation. While electron spin resonance (ESR) measurements could be used to deduce the presence of polarons vs bipolarons[41,42], the minimum bipolaron delocalization length with respect to the minimum polaron delocalization length remains unknown. Does a bipolaron encompass two (or more) neighboring polymer sites or does it condense two carriers into a single site?[19,33] If the latter is true then the intrinsic maximum bipolaronic charge density is $2 \times S_N$ and the volume expansion (ie. $V_{Average}$) must take into account the volume of two counterions per site (Supporting Information Figure S3). If the bipolarons delocalize across two polymer sites then Equation 2 holds true. This is still an oversimplification, as there may be a distribution of polaron and bipolaron coherence lengths which is likely dependent on the polaron density. Future studies are needed to address these questions. For this study, we assume that each site is either neutral or contains one polaron (one charge carrier) because all of the experimental evidence indicates that no bipolarons are present in these samples.

Figure 1e illustrates the processes that occur during solution sequential doping and highlights the increase in film volume and subsequent decrease in maximum site density as a result of doping. Starting with a neutral polymer film with film thickness T_N, as the film is exposed to a dopant solution, the dopants undergo charge transfer with intrinsic polymer sites while solvent molecules (ie. acetonitrile (AN)) and dopant anions diffuse into the film, resulting in a swollen film with thickness T_{swol}. Next, the film and substrate are removed from the doping solution. When the solvent evaporates, the film collapses to a doped film thickness T_D, where $T_{swol} > T_D > T_N$.[39] Since the site volume increases and the total number of sites is fixed, the resulting doped film has a reduced polymer site density (S_D).

Thermodynamics of Doping

This section demonstrates that the doping level in a film can be accurately predicted from the concentration of dopants in the doping solution. The Langmuir doping model reduces the complexity of the sequential doping process to a single equilibrium constant. Since an equilibrium constant is a thermodynamic variable, we are able to calculate the free energy of doping and to compare that to the electrochemical potential difference defined by the difference between the IE of the neutral polymer and EA of the neutral dopant. Finally, the optical data shows that the polaron mole fraction reaches a saturation point that is less than complete doping. We discuss and quantify the implications of doping saturation from a bulk thermodynamic perspective.

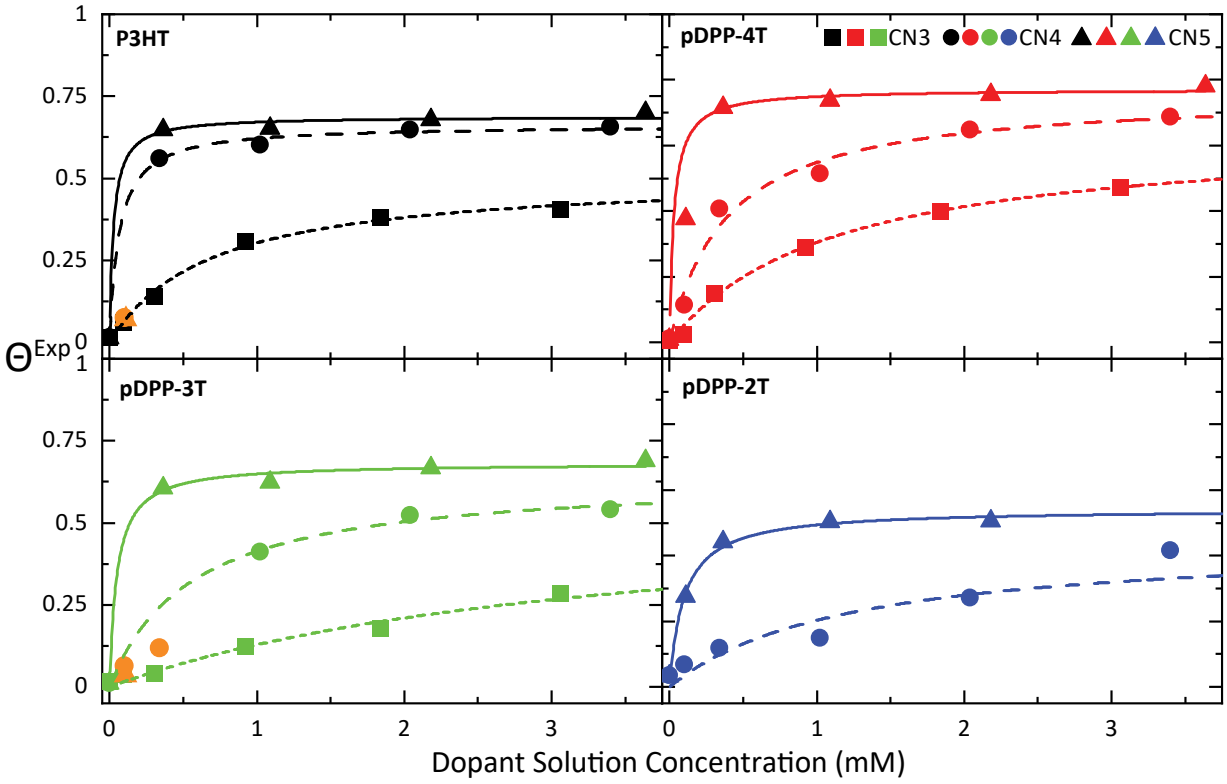

Figure 2: **Langmuir Isotherm:** Experimental polaron mole fraction (Θ^{Exp}) determined from our previously reported UV-Vis-NIR analysis.[28] Data is fit using the Langmuir doping model in Equation 3. The low C_{sol} points marked in orange were excluded from the fit.

Figure 2 shows the measured change in Θ as a function of the dopant solution concentration (C_{sol}) for all eleven studied polymer/dopant systems. The Θ values are directly deduced from the UV-vis-NIR absorbance spectra of the doped films, as previously reported.[28] All of the polymers show similar trends. As C_{sol} increases, Θ increases until reaching a saturated polaron mole fraction (Θ_{sat}). As the polymer/dopant $|\Delta E|$ increases from the CN3 to the CN5 dopant, Θ_{sat} also increases. Another clear trend is that, for the DPP polymers, Θ reaches saturation at a lower C_{sol} for higher $|\Delta E|$ dopants. This indicates that the polymer/dopant combinations with higher $|\Delta E|$ result in a higher ratio of ionized polymer sites at identical dopant concentrations. Somewhat unexpectedly, the P3HT film reaches a lower Θ_{sat} than the pDPP-4T film, even though P3HT has the lowest IE of the studied polymers and the largest $|\Delta E|$ with each of the studied dopants. We hypothesize that this may be related to differing entropic effects between the P3HT and pDPP films upon doping, which is associated with dramatically broader DOS distributions in P3HT compared to the pDPP polymers. The pDPP polymers are rigid, rod-like co-polymers with significantly less dihedral disorder than P3HT chains. We note this result is fully consistent with published observations that reduction of polymer dihedral disorder increases charge mobility in both neutral and charged polymers.[26,43]

As previously reported,[28] doping with CN3, CN4, or CN5 bleaches the optical absorbance associated with crystalline P3HT domains, while the broad, blue-shifted absorbance from amorphous P3HT remains essentially unchanged upon doping. Since P3HT has a significantly larger distribution of amorphous domains compared to the DPP polymers, there is a larger population of P3HT sites that remain neutral after exposure to the dopant solution. If we consider that amorphous (blue-shifted) sites represent a different DOS distribution, then the electrons located at the HOMO of the amorphous P3HT sites have a less favorable energetic potential for charge transfer than the electrons located at the HOMO of the crystalline sites. In short, ΔE provides insight into whether charge transfer will occur between a given polymer/dopant pair, but knowledge of the DOS distribution, that is, of its width,

shape, and gap states, is required to predict the experimental Θ for a given system.[44]

The presented Langmuir Isotherm model (LIM) is particularly useful because it is obtained independently of DOS parameters and provides thermodynamic equilibrium information on the doping reaction. The data in Figure 2 is experimentally obtained using the non-interacting site model[28] and fit using an altered LIM (Equation 3).[24,45] The LIM is conventionally used to account for the filling of a surface with non-interacting particles, for example N_2 on a porous oxide.[46] This model translates well to a sequentially doped polymer film, since the film is formed prior to doping there are a fixed number of polymer sites that can either be occupied (doped) or unoccupied (neutral) by molecular dopants. Since we have no spectroscopic evidence of bipolaron formation in these samples, the LIM is simplified to

$$\frac{N_{polaron}}{N_{neutral} + N_{polaron}} = \Theta = \Theta_{sat} \frac{K_{eq} C_{sol}}{1 + K_{eq} C_{sol}} \tag{3}$$

where K_{eq} is the equilibrium constant for doping between the solution phase dopant and solvent swollen polymer film. Figure 2 shows that the LIM fits the concentration dependence of Θ for all the explored polymer/dopant combinations. Thus, the LIM delivers high value thermodynamic information that is otherwise missing in the literature: It provides a relatively simple means to quantitatively compare the efficacy of solution doping of a particular polymer with a particular molecular dopant in a particular solvent as a function of concentration. With the extraction of K_{eq}, the LIM enables direct, quantifiable comparisons between different polymers and different dopants under different processing conditions. Table 2 lists the ΔE, K_{eq}, Θ_{sat}^{Exp}, and free energy of doping ΔG_L°.ΔG_L° is obtained using Equation 4 with K_{eq} in units of M^{-1}. Since this model removes 'undopable' sites by fitting to a saturation level, ΔG_L° corresponds to the equilibrium doping between accessible polymer sites and the dopants.

$$\Delta G_L^\circ = RT \ln(K_{eq}) \tag{4}$$

Table 2: Experimental ΔE, K_{eq}, ΔG_L°, and Θ_{sat} for each polymer and dopant.

Polymer	**Dopant**	ΔE from CV (eV)	$K_{eq}(\mathrm{mM}^{-1})$	ΔG_L° (eV)	Θ_{sat}^{Exp}
P3HT	CN3	-0.4	1.46	-0.19	0.51 ±0.02
	CN4	-0.51	15.33	-0.25	0.66 ±0.02
	CN5	-0.65	38.1	-0.27	0.69 ±0.02
pDPP-4T	CN3	-0.24	0.89	-0.17	0.65 ±0.02
	CN4	-0.35	2.59	-0.20	0.76 ±0.02
	CN5	-0.49	33	-0.27	0.77 ±0.02
pDPP-3T	CN3	-0.18	0.49	-0.16	0.41 ±0.1
	CN4	-0.29	1.79	-0.19	0.64 ±0.02
	CN5	-0.43	19.8	-0.25	0.68 ±0.02
pDPP-2T	CN4	-0.28	0.83	-0.17	0.45 ±0.1
	CN5	-0.42	10.2	-0.24	0.54 ±0.02

To demonstrate that the LIM results in consistent trends between polymers, we plotted the thermodynamic parameters extracted from the LIM fits in Figure 3. For all four polymers, Θ_{sat} saturates with respect to ΔE (Figure 3a). This indicates that simply increasing the energetic driving force for doping is not an effective strategy for reaching 100% polaron population (i.e. $\Theta = 1$), and that the upper doping limit for sequential doping is controlled by additional factors that are not accounted for in the idealized model. For example, polymer end groups, coiled configurations, and dihedral bends can lead to configurations that cannot support a polaron.[26] The group of Brinkmann has demonstrated that alignment of the polymer chains reduces the defect density, which should increase Θ_{sat} significantly.[12,47]

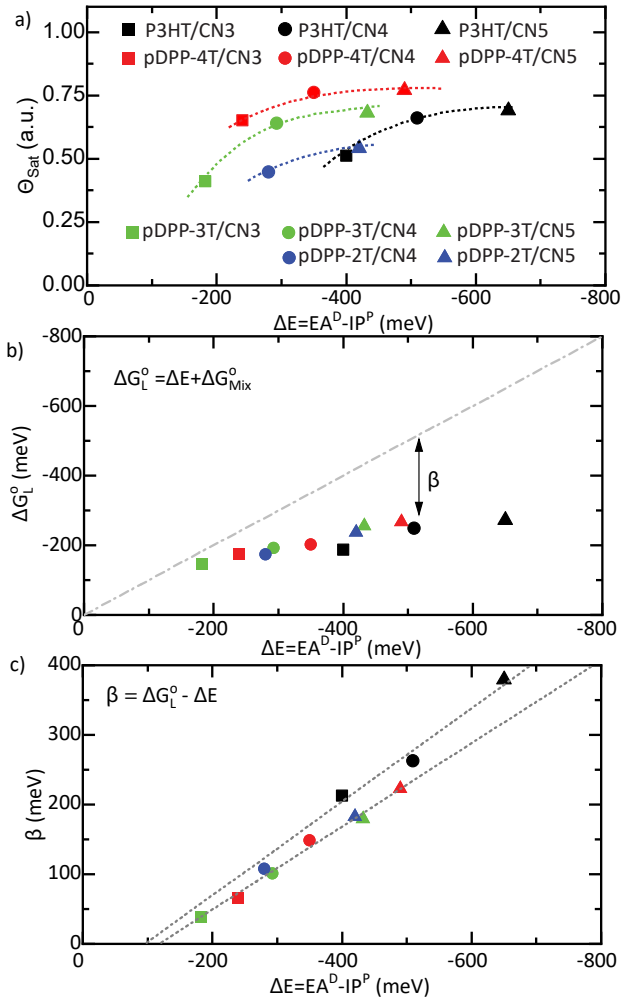

Figure 3: **Thermodynamic Parameters:** a) The saturated polaron mole fraction (Θ_{sat}) and b) the ΔG°_{L} obtained from the Langmuir Isotherm fits plotted against the chemical potential for doping (ΔE). c) The energy loss (β) from solution sequential doping, extracted from b). Dotted lines indicate systematically higher β for P3HT than for the DPP polymers.

Figure 3b shows ΔG°_{L} vs ΔE for all eleven dopant/polymer pairs. For all measured polymer/dopant pairs, ΔG°_{L} is negative, therefore doping is spontaneous. This plot shows that the magnitude of the free energy of doping increases linearly with increased ΔE, with a slope of only 0.40, indicating that increasing the EA of the dopant does not yield a one to one increase in the energetic driving force for doping.[48] The grey dashed line represents the expected change in the free energy assuming that doping is controlled entirely by ΔE (i.e.: $\Delta G^{\circ}_{L} = \Delta E$). As alluded to above, this energy loss is associated with a combination

of mechanisms including the reorganization energy,[49] the free energies of mixing (between the polymer, the processing solvent, and the molecular dopants), and entropic effects from structural rearrangements. Figure 3c shows the energy loss ($\beta = \Delta G_L^\circ - \Delta E$) upon doping, i.e., the difference between the expected energetic driving force and the free energy change from the LIM. Interestingly, β also increases linearly, indicating that increasing ΔE leads to a proportional energy loss in solution sequential doping. It is yet unreported whether solution doping is an adiabatic or non-adiabatic process and may be dependent on the doping process, i.e., mixed in solution vs sequential. In addition to the factors mentioned above, energy loss is likely also related to heat released during the doping reaction, which is then transferred into the bulk substrate and doping solution. Therefore, β is a function of the enthalpy of mixing, the entropy of mixing, and the heat produced during the reaction. Further thermodynamic studies are needed to elucidate the direct relationship between these parameters. We note that extrapolating the linear relationship between β and ΔE to $\beta = 0$ indicates that the energy loss onset is at a value of $\Delta E = -0.11 \pm 0.01eV$. This suggests that the onset of molecular doping can be achieved with a ΔE of ≈ 0.11 eV but will be limited to a near zero saturated doping level ($\Theta_{sat} \approx 0$). To obtain higher doping levels, i.e., extracting electrons from deeper within the DOS, a stronger dopant is needed. The parameter β demonstrates that both homopolymers and alternating co-polymers, despite their varying levels of crystallinity, require the same increase in chemical doping driving force ΔE to achieve the same increase in ΔG_L°.

Density of States

The above analysis presents a site model that enables prediction of the doping level in a polymer controlled by an equilibrium. We determine a thermodynamic equilibrium between dopants and the "available" polymer sites and present a free energy for doping. If this site model is correct, then it should be possible to obtain a self-consistent density of states model that is consistent with semiconductor theory and quantitatively matches both optical and

electrical measurements. To quantify the importance of considering the full DOS profile, we computationally modeled the occupation of the DOS in all SP:dopant systems. We followed the approach demonstrated by Oehzelt et al., who developed a self-consistent electrostatic model that determines the Fermi level as well as energy level alignments between organic semiconductors and substrate materials.[50] The model describes the organic semiconductor band edge and gap states, which makes it accurate for multiple applications.[5,51,52] A solution for the position of the Fermi level as well as for the polaron density (occupation of the SP HOMO) and anion density (occupation of the dopant LUMO) is simultaneously obtained using an iterative procedure. The procedure assumes a trial value for the Fermi level, then the occupation of the frontier energy levels is obtained for the SP's HOMO and the dopant's LUMO using the following equations:

$$\rho_{SP} = C_{SP} \int_{-\infty}^{+\infty} \frac{1}{\frac{1}{2} e^{-\frac{(E-E_{\mathrm{F}})}{k_B T}} + 1} \cdot g(E + V(z)) dE, \tag{5}$$

$$\rho_{D} = C_{D} \int_{-\infty}^{+\infty} \frac{1}{\frac{1}{2} e^{+\frac{(E-E_{\mathrm{F}})}{k_B T}} + 1} \cdot g(E + V(z)) dE, \tag{6}$$

where ρ_{SP} is the charge density in the SP's HOMO (the occupation of its LUMO is negligible), ρ_D the charge density in the dopant's LUMO (the occupation of its HOMO is negligible), C_{SP} and C_D are the SP and dopant concentrations respectively, E is the energy corresponding to an anion or polaron state, E_F is the Fermi level, k_B is Boltzmann's constant, and T is the temperature. The DOS is represented by a Gaussian function, defined by its center and σ, the full width at half maximum (FWHM). σ_{HOMO} locates the SP's IE and σ_{LUMO} the dopant's EA at two times σ from the DOS center. For simplicity, we obtained the relative intensity and width of the Gaussian DOS for each SP in this model directly from the fit to the 0-0 UV-vis-NIR absorbance band used to determine the polaron mole fraction.[28] The position of the Gaussian edge was determined using CV measurements. For the dopants, the DOS width is taken to be 0.05 eV, a value which was previously used to model TCNQ

and its fluorinated derivatives to predict doping levels in solution mixed dopants/SPs[44,53]. These assumptions mean that all of the parameters used for the DOS model come directly from measured data. $V(z)$ describes the electric potential between discretization intervals in the out-of-plane direction, i.e., along the material thickness, making ρ_{SP} and ρ_{dopant} also functions of z. Charges obtained from Equations 5 and 6 are then used to solve the discretized Poisson equation for the electrostatic potential in one dimension (with mixed Dirichlet and Neumann boundary conditions):

$$\nabla[\varepsilon(z)\nabla V(z)] = -\frac{\rho(z)}{\varepsilon_0}, \tag{7}$$

where $\varepsilon(z)$ is the permittivity of the material within each discretization interval and ε_0 is the permittivity of vacuum. The calculated potential is used to shift the Fermi level position, and the process is iterated until the system is physically accurate, i.e., until it is overall neutral. Since there are no conducting electrodes accounted for in the modeling, the system is assumed to be isotropic in z and the discretization parameters do not matter, as the solution is independent from them.

The model is illustrated in Figure 4. The positions of the data-derived frontier energy levels of all compounds are plotted in Figure 4a. Figures 4b and 4c show the simulated shift of the Fermi level as a function of the dopant concentration for pDPP-3T/CN4 and pDPP-4T/CN5, respectively. These systems were chosen for discussion because they highlight two cases where the extremum of the dopants unoccupied DOS is located above and below the extremum of the polymers occupied DOS. The change in Fermi energy is projected inside the DOS of the pristine SP. When no dopants are present, the Fermi levels are found at mid-position between the HOMO and LUMO of the SP (above the limits of the figure). As the dopant concentration increases, the Fermi level is gradually pushed into the occupied DOS of the SP, leading to increasingly significant ionization levels. For all systems the dopant density is increased until the dopant concentration reaches one dopant molecule per SP repeating unit. The theoretical saturated polaron mole fraction (Θ_{Sat}^{Theory}) is extracted

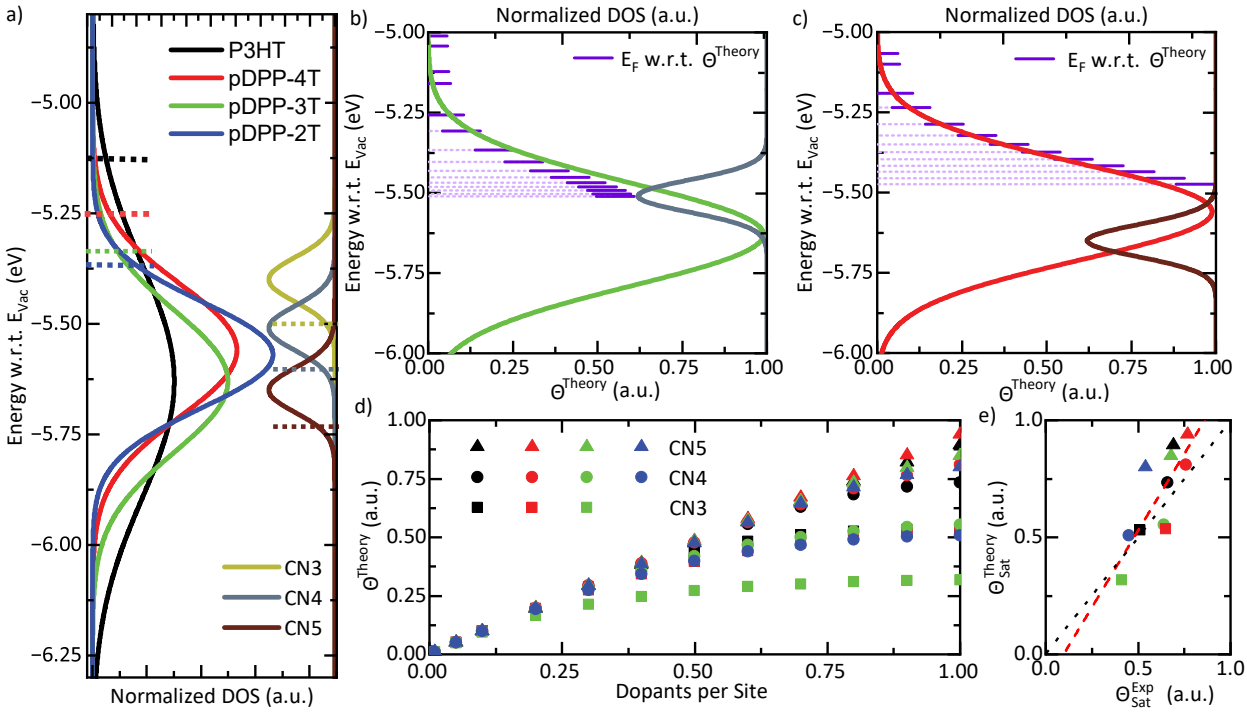

Figure 4: **Density of States Model:** a) The occupied DOS for the four polymers and the unoccupied DOS for the three dopants evaluated in this study. b) Evolution of the Fermi level (purple steps) for pDPP-3T doped with CN4 as a function of the computational polaron mole fraction (Θ^{Theory}), projected onto the pristine occupied and unoccupied DOS of the pDPP-3T and CN4. c) Evolution of the Fermi level (purple steps) for pDPP-4T doped with CN5 as a function of the Θ^{Theory}, projected onto the pristine occupied and unoccupied DOS of the pDPP-4T and CN5. d) Θ^{Theory} with respect to the number of dopants per polymer site. e) A linear relationship between the theoretical saturated polaron mole fraction (Θ_{Sat}^{Theory}) and experimentally obtained saturated polaron mole fraction (Θ_{Sat}^{Exp}). The linear fit of the data is shown in red, while the dotted black line shows the ideal 1:1 correspondence for reference.

from the calculation where the dopant density matches the SP monomer density, i.e. one dopant per site. The IE of the SP alone is not a reliable predictor of the saturated doping levels because, as shown in Figures 4b and 4c, the Fermi level moves within the DOS of the intrinsic SP. Therefore, the occupation of the DOS at high dopant concentrations depends on the curvature of the frontier orbital and not solely on its edge position. For this reason, σ_{HOMO} is a crucial parameter describing the filling of the DOS, since, as described above and illustrated in Figure 4a, the DOS of the SPs all feature different σ values and total state densities. All parameters used for modelling the occupation of the DOS are provided in Table 3.

Table 3: Parameters extracted from modelling the occupation of the DOS in the different systems in units of eV. C^P and C^D refer to the Gaussian center of the SP and the dopant DOS respectively, i.e. to the maximum of the distribution. IE and EA refer to the edge of the SP and dopant Gaussian DOS respectively, located at 2σ from the maximum. E_F^{sat} is the solution found for the energy corresponding to the Fermi level at saturation.

Polymer	Dopant	IE	C^P	σ_{OSC}	EA	C^D	σ_{dopant}	E_F^{sat}
P3HT	CN3	-5.10	-5.63	0.265	-5.50	-5.40	0.05	-5.40
P3HT	CN4	-5.10	-5.63	0.265	-5.61	-5.51	0.05	-5.47
P3HT	CN5	-5.10	-5.63	0.265	-5.75	-5.65	0.05	-5.51
pDPP-4T	CN3	-5.26	-5.56	0.15	-5.50	-5.40	0.05	-5.40
pDPP-4T	CN4	-5.26	-5.56	0.15	-5.61	-5.51	0.05	-5.45
pDPP-4T	CN5	-5.26	-5.56	0.15	-5.75	-5.65	0.05	-5.47
pDPP-3T	CN3	-5.31	-5.63	0.16	-5.50	-5.40	0.05	-5.44
pDPP-3T	CN4	-5.31	-5.63	0.16	-5.61	-5.51	0.05	-5.51
pDPP-3T	CN5	-5.31	-5.63	0.16	-5.75	-5.65	0.05	-5.58
pDPP-2T	CN4	-5.33	-5.57	0.12	-5.61	-5.51	0.05	-5.52
pDPP-2T	CN5	-5.33	-5.57	0.12	-5.75	-5.65	0.05	-5.59

Figure 4d shows the predicted change in Θ as a function of the number of dopants per monomer site. This is not the same as the data fit in the LIM plots in Figure 2 because the Langmuir data depends on C_{sol} whereas Figure 4d plots the ratio of monomer sites to dopant molecules directly. For all of the SP/dopant pairs, the dopant ionization is less than 100% at high dopant/site ratios because the change in Fermi energy prevents further doping, leading to a saturation of the Θ_{sat}^{Theory}. To check the quantitative agreement between the DOS model the measured data, we plot Θ_{sat}^{Theory} vs Θ_{sat}^{Exp} in Figure 4e. If the data and theory matched, all points would lie on the diagonal dotted black line. This shows that the DOS model predicts Θ_{sat}^{Exp} to within a 32% deviation for worst fit samples, which is exceptionally accurate for a simplistic Gaussian DOS model with no fit parameters and experimental data that was solely determined from UV-vis-NIR and CV. A linear fit to the modeled vs experimental Θ_{sat} (red dotted line) yields an intercept of 0.12, which is nearly identical to the onset for doping predicted from Figure 3c. Both models show a similar required over-potential for the onset of doping. The slope is slightly higher than 1 (1.28), which we ascribe to the fact that the modelling of the DOS assumes that all sites are physically identical within a

Gaussian profile. In a real SP sample, it is well known that certain sites are systematically more difficult to dope including chain ends and kinks/bends in the polymer. Consideration of a more realistic DOS would require an asymmetric Gaussian or multiple Gaussian profiles that included separate populations for chain segments with various degrees of dihedral twist, i.e. straight segments, kinked segments, and chain ends. Overall, we show that the simple Gaussian DOS model populated with only measured parameters is remarkably accurate in quantitatively modeling the saturated doping levels across multiple polymers and dopants.

A second crucial check on the accuracy of the Gaussian DOS model is displayed in Figure 5a, where we plot the predicted polaron mole fraction (Θ^{Theory}) against the predicted polaron density (P^{Theory}) in units of cm^{-3}. Interestingly, all of the SP/dopant pairs show nearly the same curve, with the main differences originating from the differing molecular volumes of the SPs and dopants. Figure 5b shows the experimentally obtained polaron density (P) that is determined using Equation 2 with the experimentally obtained Θ. A visual inspection shows the predicted and measured concentration dependent P to be qualitatively the same within the measured range. The theoretical curve overestimates Θ_{sat} because the Gaussian DOS model ignores inaccessible sites, while in real samples, polymer chain ends and static disorder produce trap states and reduce the number of "dopable" sites. These plots show conclusively that the use of the optically obtained Θ values yield, within uncertainty, the same result as the DOS model. For both measured and modeled data, accurate determination of P requires accounting of the monomer density as a function of the changing film volume with increasing dopant density. The close correspondence of the measured and modeled concentration-dependent data is a powerful tool that will enable researchers to make direct and quantitative comparisons between different polymers with different dopants as a function of the doping level.

Electronic Transport

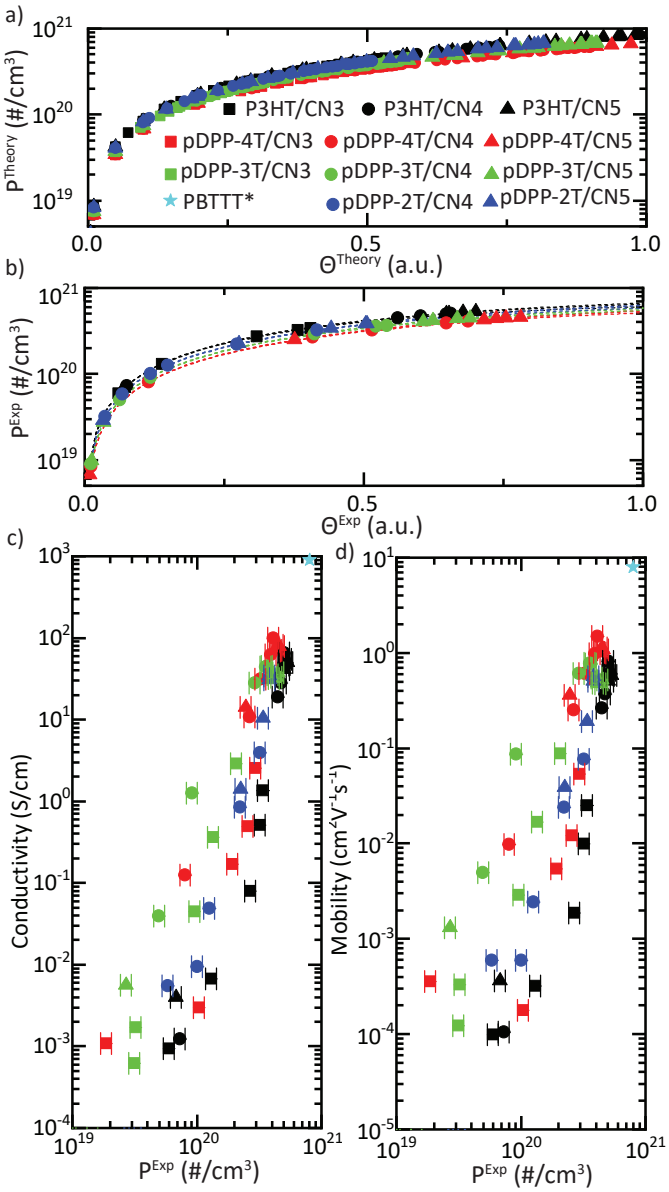

Figure 5: **Electronic Transport:** a) Hole carrier density (P^{Theory}) calculated from the occupation of the DOS with respect to the theoretical polaron mole fraction (Θ^{Theory}). b) Linearly approximated hole carrier density (P^{Exp}) from the experimental polaron mole fraction (Θ^{Exp}) (Equation 2). c) Measured conductivity and d) calculated mobility (μ) as a function of the carrier density from part b). The conductivity of sequentially doped PBTTT film is extracted from Jacobs et al.[26]

This section compares the measured electronic properties of the doped films as a function of the polaron density. The film conductivity and mobility show a greater dependence on the polaron density than the polymer or dopant identity. This demonstrates the usefulness and consistency of the presented polaron density model.

One immediate and powerful use of the polaron density model presented here is illustrating the measured conductivity, obtained from 4-point sheet resistance, of each polymer/dopant combination as a function of the hole carrier density (Figure 5c). Without quantifying P, analysis is limited to qualitative conclusions correlating greater ΔE and C_{sol} values to higher conductivities for each polymer/dopant pair. A consistent measure of P, reveals insights into the magnitude of effects that morphology, partial dopant ionization, and/or dopant size have on the electrical conductivity.[5,38,54,55]

Figure 5c shows that conductivity increases by six orders of magnitude and roughly linearly on a log/log plot for all SPs. With increased P, the conductivity data converges for all of the SPs and dopants, indicating that P is the dominant variable. Among the four polymers studied in this work, neither the polymer chemistry, disorder, or stiffness has as great of an impact as the carrier density for controlling electrical transport. For all polymer/dopant pairs, a $\sim$10$\times$ increase in polaron density causes a $\sim$5000$\times$ increase in the conductivity. At moderate doping levels, in the range of P = 10^{20} $\frac{\#}{cm^3}$, the pDPP-3T polymer exhibits the highest conductivity films, which are only $\sim$10$\times$ greater in conductivity than the least conductive material studied here, P3HT. Since the data converges at higher P, this means that P3HT has a larger slope compared to pDPP-3T on this plot. Interestingly, the recent reports[26] of highly doped PBTTT with unaligned conductivity of 1000 S/cm and doping level of 8×10^{20}cm^{-3} falls on the linear extrapolation of the data shown here. Designing new polymers and dopants with the goal to achieve further increased polaron density or bipolaron density is likely to yield further advances in conductivity.

Another important application of polaron density is the ability to determine the hole mobility (μ) using $\mu = \frac{\sigma}{e \cdot P}$, where e is the elementary charge (Figure 5d). As the carrier

concentration increases by an order of magnitude, the μ_h increases from $\sim 10^{-4}$ to $\sim 10^{0}$ $cm^2V^{-1}s^{-1}$, four orders of magnitude. This is in agreement with the recently developed Semi-localized Transport Model[31], Derewjanko et al.'s Mott-like transport model[56], and is consistent with the increased field effect mobility measured in the active channels of organic field effect transistors.[57] At low doping levels, Coulombic attraction between the positive polarons in the SP and the negatively charged counterions creates electrostatic potential energy wells that localize carriers and reduce the observed μ compared to field effect mobility in which counter charges are located on the other side of the dielectric layer. However, as the counterion density increases with the polaron density, the distance between nearest neighbor counterions is reduced and the potential wells overlap. This effectively flattens the energetic landscape and reduces the effective energy barriers for transport, resulting in an increased μ with carrier density. Projecting to the highest conductivities for sequentially doped, unaligned PBTTT, a charge density of $8\times10^{20}cm^{-3}$ would result in a μ of 7.8 $cm^2V^{-1}s^{-1}$. The recent result demonstrating a conductivity of several thousand S/cm in aligned PBTTT films[58] for the a charge density of 8×10^{20} cm^{-3} implies that the μ is approaching 25-30 $cm^2V^{-1}s^{-1}$ in highly doped and aligned films.

Conclusions

The main objective of this work is to demonstrate a simple empirical method to quantify the carrier density in highly doped conjugated polymer films and to enable quantitative comparison between different polymers and different dopants. This work builds off our previous model that determines polaron mole fractions from UV-vis-NIR data. Coupled to molar volume estimates for dopant anions, maximum carrier densities can be reduced by 25-40% due to film expansion upon doping. An adapted Langmuir Isotherm model predicts the change in polaron mole fraction as a function of the solution concentration of the dopants, demonstrating equilibrium doping levels. Conversion of the equilibrium constants to Gibbs

free energies for doping enabled determination of a sub-linear relationship between ΔE and ΔG with an offset energy equal to the overpotential needed for the onset of chemical doping. Simulating the density of states using CV and UV-vis-NIR derived Gaussian energy distributions demonstrates the same predicted overpotential offset and consistent prediction of the film polaron density for all polymers and dopants. The close match between empirical data and predictions for both thermodynamic and DOS models demonstrates that this empirical method can be consistently applied and used for doped and electrochemically doped semiconducting polymer films.

Secondly, increasing polaron density yields exponential increases in film conductivity and mobility for all polymer dopant pairs. Polymer identity has a minor affect on conductivity as polaron densities approach their maximum theoretical limit. We demonstrate up to 80% polymer sites were doped; higher polaron densities in these polymer/dopant pairs was not possible because (1) the monomer density is reduced by the addition of dopant anions, (2) the maximum Fermi energy shift is limited by the DOS distributions of the polymer/dopant pairs, and (3) the presence of high dihedral-torsion sites and chain ends produce deep energy trap states that are inaccessible to the dopants and not accounted for using a single Gaussian DOS model. The hole mobility increases linearly on a log/log plot with increased polaron density for all polymer/dopant pairs, showing that the mobility is a strong function of carrier density in organic electronic materials. This result suggests that in order to obtain higher conductivity films future synthetic efforts should focus on increasing polaron density by designing (1) monomers with shorter side chains, (2) polymer backbones that have a shorter minimum polaron (bipolaron) delocalization lengths, (3) and smaller multivalent dopant counterions.

Conflicts of Interest

There are no conflicts of interest to declare.

Acknowledgments

The majority of this work was funded by the National Science foundation award #1804690, including salary for AJM, TLM, and GG. This work benefited from a UC Davis Grant to Promote New Research Initiatives and Collaborative Interdisciplinary Research. This research was enabled in part by by Calcul Québec (calculquebec.ca) and the Digital Research Alliance of Canada (alliancecan.ca). IS and MBR acknowledges financial support by NSERC (funding Reference Nos. RGPIN-201805092), the Fonds de recherche du Québec-Nature et technologies (FRQNT) (funding Reference No. 2020-NC-271447), and Concordia University. Work in Princeton was supported by Grant No. 2018349 from the United States-Israel Binational Science Foundation (BSF).

References

(1) Yu, P. Y.; Cardona, M. *Fundamentals of semiconductors physics and materials properties*; Springer, 2010.

(2) Shklovskii, B. I.; Efros, A. L. *Electronic properties of doped semiconductors*; Springer-Verlag, 1984.

(3) Plummer, J.; Griffin, P. Material and process limits in silicon VLSI technology. *Proceedings of the IEEE* **2001**, *89*, 240–258.

(4) Jacobs, I. E.; Moulé, A. J. Controlling Molecular Doping in Organic Semiconductors. *Advanced Matererials* **2017**, *29*, 1703063–n/a.

(5) Salzmann, I.; Heimel, G.; Oehzelt, M.; Winkler, S.; Koch, N. Molecular Electrical Doping of Organic Semiconductors: Fundamental Mechanisms and Emerging Dopant Design Rules. *Accounts of Chemical Research* **2016**, *49*, 370–378.

(6) Scaccabarozzi, A.; Basu, A.; Aniés, F.; Liu, J.; Zapata-Arteaga, O.; Warren, R.; Firdaus, Y.; Nugraha, M.; Lin, Y.; Campoy-Quiles, M.; Koch, N.; Müller, C.; Tsetseris, L.; Heeney, M.; Antholoulos, T. D. Doping approaches for organic semiconductors. *Chemical Reviews* **2021**, *122*, 4420–4492.

(7) Patel, S. N.; Chabinyc, M. L. Anisotropies and the thermoelectric properties of semiconducting polymers. *Journal of Applied Polymer Science* **2017**, *134*, 44403.

(8) Hofmann, A. I.; Kroon, R.; Zokaei, S.; Järsvall, E.; Malacrida, C.; Ludwigs, S.; Biskup, T.; Müller, C. Chemical Doping of Conjugated Polymers with the Strong Oxidant Magic Blue. *Advanced Electronic Materials* **2020**, *6*, 2000249.

(9) Kang, K.; Watanabe, S.; Broch, K.; Sepe, A.; Brown, A.; Nasrallah, I.; Nikolka, M.; Fei, Z.; Heeney, M.; Matsumoto, D.; Marumoto, K.; Tanaka, H.; Kuroda, S.; Sirringhaus, H. 2D coherent charge transport in highly ordered conducting polymers doped by solid state diffusion. *Nat. Mater.* **2016**, *15*, 896–902.

(10) Kao, C. Y.; Lee, B.; Wielunski, L. S.; Heeney, M.; McCulloch, I.; Garfunkel, E.; Feldman, L. C.; Podzorov, V. Doping of Conjugated Polythiophenes with Alky Silanes. *Adv. Funct. Mater.* **2009**, *19*, 1906–1911.

(11) Jacobs, I. E. et al. High-Efficiency Ion-Exchange Doping of Conducting Polymers. *Advanced Materials 34*, 2102988.

(12) Vijayakumar, V.; Zhong, Y.; Untilova, V.; Bahri, M.; Herrmann, L.; Biniek, L.; Leclerc, N.; Brinkmann, M. Bringing Conducting Polymers to High Order: Toward Conductivities beyond 105 S cm1 and Thermoelectric Power Factors of 2 mW m1 K2. *Adv. Energy Mater.* **2019**, *9*, 1900266.

(13) Yamashita, Y.; Tsurumi, J.; Ohno, M.; Fujimoto, R.; Kumagai, S.; Kurosawa, T.; Okamoto, T.; Takeya, J.; Watanabe, S. Efficient molecular doping of polymeric semiconductors driven by anion exchange. *Nature* **2019**, *572*, 634–638.

(14) Kim, G.-H.; Shao, L.; Zhang, K.; Pipe, K. P. Engineered doping of organic semiconductors for enhanced thermoelectric efficiency. *Nature Materials* **2013**, *12*, 719–723.

(15) Ghosh, R.; Spano, F. C. Excitons and Polarons in Organic Materials. *Acc. Chem. Res.* **2020**, *53*, 2201–2211.

(16) Ghosh, R.; Pochas, C. M.; Spano, F. C. Polaron Delocalization in Conjugated Polymer Films. *J. Phys. Chem. C* **2016**, *120*, 11394–11406.

(17) Ghosh, R.; Chew, A. R.; Onorato, J.; Pakhnyuk, V.; Luscombe, C. K.; Salleo, A.; Spano, F. C. Spectral Signatures and Spatial Coherence of Bound and Unbound Polarons in P3HT Films: Theory Versus Experiment. *J. Phys. Chem. C* **2018**, *122*, 18048–18060.

(18) Ghosh, R.; Luscombe, C. K.; Hambsch, M.; Mannsfeld, S. C. B.; Salleo, A.; Spano, F. C. Anisotropic Polaron Delocalization in Conjugated Homopolymers and Donor–Acceptor Copolymers. *Chem. Mater.* **2019**, *31*, 7033–7045.

(19) Qarai, M. B.; Ghosh, R.; Spano, F. C. Understanding Bipolarons in Conjugated Polymers Using a Multiparticle Holstein Approach. *J. Phys. Chem. C* **2021**, *125*, 24487–24497.

(20) Voss, M. G.; Challa, J. R.; Scholes, D. T.; Yee, P. Y.; Wu, E. C.; Liu, X.; Park, S. J.; León Ruiz, O.; Subramaniyan, S.; Chen, M.; Jenekhe, S. A.; Wang, X.; Tolbert, S. H.; Schwartz, B. J. Driving Force and Optical Signatures of Bipolaron Formation in Chemically Doped Conjugated Polymers. *Advanced Materials* **2021**, *33*, 2000228.

(21) Kiefer, D. et al. Double Doping of Conjugated Polymers with Monomer Molecular Dopants. *Nature Materials* **2019**, *18*, 149–155.

(22) Tsokkou, D.; Cavassin, P.; Rebetez, G.; Banerji, N. Bipolarons rule the short-range

terahertz conductivity in electrochemically doped P3HT. *Mater. Horiz.* **2022**, *9*, 482–491.

(23) Stanfield, D. A.; Mehmedović, Z.; Schwartz, B. J. Vibrational Stark Effect Mapping of Polaron Delocalization in Chemically Doped Conjugated Polymers. *Chemistry of Materials* **2021**, *33*, 8489–8500.

(24) Jacobs, I. E.; Aasen, E. W.; Oliveira, J. L.; Fonseca, T. N.; Roehling, J. D.; Li, J.; Zhang, G. W.; Augustine, M. P.; Mascal, M.; Moulé, A. J. Comparison of solution-mixed and sequentially processed P3HT:F4TCNQ films: effect of doping-induced aggregation on film morphology. *Journal of Materials Chemistry C* **2016**, *4*, 3454–3466.

(25) Untilova, V.; Hynynen, J.; Hofmann, A. I.; Scheunemann, D.; Zhang, Y. D.; Barlow, S.; Kemerink, M.; Marder, S. R.; Biniek, L.; Muller, C.; Brinkmann, M. High Thermoelectric Power Factor of Poly(3-hexylthiophene) through In-Plane Alignment and Doping with a Molybdenum Dithiolene Complex. *Macromolecules* **2020**, *53*, 6314–6321.

(26) Jacobs, I. E. et al. Structural and dynamic disorder, not ionic trapping, controls charge transport in highly doped conducting polymers. *Journal of the American Chemical Society* **2022**, *144*, 3005–3019.

(27) Yi, H. T.; Gartstein, Y. N.; Podzorov, V. Charge carrier coherence and hall effect in organic semiconductors. *Scientific Reports* **2016**, *6*, 23650.

(28) Moulé, A. J.; Gonel, G.; Murrey, T. L.; Ghosh, R.; Saska, J.; Shevchenko, N. E.; Denti, I.; Fergerson, A. S.; Talbot, R. M.; Yacoub, N. L.; Mascal, M.; Salleo, A.; Spano, F. C. Quantifying Polaron Mole Fractions and Interpreting Spectral Changes in Molecularly Doped Conjugated Polymers. *Advanced Electronic Materials* **2022**, *8*, 2100888.

(29) Balooch Qarai, M.; Chang, X.; Spano, F. C. Vibronic exciton model for low bandgap donor–acceptor polymers. *J. Chem. Phys.* **2020**, *153*, 244901.

(30) Yee, P. Y.; Scholes, D. T.; Schwartz, B. J.; Tolbert, S. H. Dopant-Induced Ordering of Amorphous Regions in Regiorandom P3HT. *The Journal of Physical Chemistry Letters* **2019**, *10*, 4929–4934.

(31) Gregory, S. A.; Hanus, R.; Atassi, A.; Rinehart, J. M.; Wooding, J. P.; Menon, A. K.; Losego, M. D.; Snyder, G. J.; Yee, S. K. Quantifying charge carrier localization in chemically doped semiconducting polymers. *Nature Materials* **2021**, *20*, 1414–1421.

(32) Thorley, K. J. Estimation of Polaron Delocalization Lengths in Conjugated Organic Polymers. *The Journal of Physical Chemistry B* **2023**, *127*, 5102–5114, PMID: 37220398.

(33) Wu, E. C.; Salamat, C. Z.; Ruiz, O. L.; Qu, T.; Kim, A.; Tolbert, S. H.; Schwartz, B. J. Counterion Control and the Spectral Signatures of Polarons, Coupled Polarons, and Bipolarons in Doped P3HT Films. *Advanced Functional Materials* **2023**, *33*, 2213652.

(34) Untilova, V.; Zeng, H. Y.; Durand, P.; Herrmann, L.; Leclerc, N.; Brinkmann, M. Intercalation and Ordering of F(6)TCNNQ and F(4)TCNQ Dopants in Regioregular Poly(3-hexylthiophene) Crystals: Impact on Anisotropic Thermoelectric Properties of Oriented Thin Films. *Macromolecules* **2021**, *54*, 6073–6084.

(35) Wegner, B.; Grubert, L.; Dennis, C.; Opitz, A.; Röttger, A.; Zhang, Y.; Barlow, S.; Marder, S. R.; Hecht, S.; Müllen, K.; Koch, N. Predicting the yield of ion pair formation in molecular electrical doping: redox-potentials versus ionization energy/electron affinity. *Journal of Matererials Chemistry C* **2019**, *7*, 13839–13848.

(36) Saska, J.; Shevchenko, N. E.; Gonel, G.; Bedolla-Valdez, Z. I.; Talbot, R. M.; Moulé, A. J.; Mascal, M. Synthesis and characterization of solution processable, high electron affinity molecular dopants. *J. Mater. Chem. C* **2021**, *9*, 15990–15997.

(37) Chen, C. et al. Observation of Weak Counterion Size Dependence of Thermoelectric Transport in Ion Exchange Doped Conducting Polymers Across a Wide Range of Con-

ductivities. *Advanced Energy Materials* **2023**, *13*, Chen, Chen Jacobs, Ian E. Kang, Keehoon Lin, Yue Jellett, Cameron Kang, Boseok Lee, Seon Baek Huang, Yuxuan Qarai, Mohammad Balooch Ghosh, Raja Statz, Martin Wood, William Ren, Xinglong Tjhe, Dion Sun, Yuanhui She, Xiaojian Hu, Yuanyuan Jiang, Lang Spano, Frank C. McCulloch, Iain Sirringhaus, Henning Statz, Martin/IUN-6429-2023; McCulloch, Iain/G-1486-2015; Hu, Yuanyuan/J-5017-2016 Statz, Martin/0000-0001-7791-3981; McCulloch, Iain/0000-0002-6340-7217; Wood, William Alexander/0000-0003-2451-0614; Hu, Yuanyuan/0000-0001-8511-1401 1614-6840.

(38) Thomas, E. M.; Peterson, K. A.; Balzer, A. H.; Rawlings, D.; Stingelin, N.; Segalman, R. A.; Chabinyc, M. L. Effects of Counter-Ion Size on Delocalization of Carriers and Stability of Doped Semiconducting Polymers. *Adv. Electron. Mater.* **2020**, *6*, 2000595.

(39) Murrey, T. L.; Guo, K.; Mulvey, J. T.; Lee, O. A.; Cendra, C.; Bedolla-Valdez, Z. I.; Salleo, A.; Moulin, J.-F.; Hong, K.; Moulé, A. J. Additive solution deposition of multilayered semiconducting polymer films for design of sophisticated device architectures. *J. Mater. Chem. C* **2019**, *7*, 953–960.

(40) ChemAxon MarvinSketch 19.21.5. 2020.

(41) Bredas, J. L.; Street, G. B. Polarons, bipolarons, and solitons in conducting polymers. *Accounts of Chemical Research* **1985**, *18*, 309–315.

(42) Voss, M. G.; Challa, J. R.; Scholes, D. T.; Yee, P. Y.; Wu, E. C.; Liu, X.; Park, S. J.; León Ruiz, O.; Subramaniyan, S.; Chen, M.; Jenekhe, S. A.; Wang, X.; Tolbert, S. H.; Schwartz, B. J. Driving Force and Optical Signatures of Bipolaron Formation in Chemically Doped Conjugated Polymers. *Advanced Materials* **2021**, *33*, 2000228.

(43) Venkateshvaran, D. et al. Approaching disorder-free transport in high-mobility conjugated polymers. *Nature* **2014**, *515*, 384–8.

(44) Hase, H.; Berteau-Rainville, M.; Charoughchi, S.; Orgiu, E.; Salzmann, I. Doping-related broadening of the density of states governs integer-charge transfer in P3HT. *Applied Physics Letters* **2021**, *118*, 203301.

(45) Murrey, T. L.; Riley, M. A.; Gonel, G.; Antonio, D. D.; Filardi, L.; Shevchenko, N.; Mascal, M.; Moule, A. J. Anion Exchange Doping: Tuning Equilibrium to Increase Doping Efficiency in Semiconducting Polymers. *J. Phys. Chem. Lett.* **2021**, *12*, 1284–1289.

(46) Kruk, M.; Jaroniec, M.; Sayari, A. Application of large pore MCM-41 molecular sieves to improve pore size analysis using nitrogen adsorption measurements. *Langmuir* **1997**, *13*, 6267–6273.

(47) Hamidi-Sakr, A.; Biniek, L.; Bantignies, J. L.; Maurin, D.; Herrmann, L.; Leclerc, N.; Leveque, P.; Vijayakumar, V.; Zimmermann, N.; Brinkmann, M. A Versatile Method to Fabricate Highly In-Plane Aligned Conducting Polymer Films with Anisotropic Charge Transport and Thermoelectric Properties: The Key Role of Alkyl Side Chain Layers on the Doping Mechanism. *Advanced Functional Materials* **2017**, *27*, 1700173.

(48) Arvind, M.; Tait, C. E.; Guerrini, M.; Krumland, J.; Valencia, A. M.; Cocchi, C.; Mansour, A. E.; Koch, N.; Barlow, S.; Marder, S. R.; Behrends, J.; Neher, D. Quantitative analysis of doping-induced polarons and charge-transfer complexes of poly(3-hexylthiophene) in solution. *The Journal of Physical Chemistry B* **2020**, *124*, 7694–7708.

(49) Marcus, R. A. On the Theory of Electron-Transfer Reactions. VI. Unified Treatment for Homogeneous and Electrode Reactions. *The Journal of Chemical Physics* **1965**, *43*, 679–701.

(50) Oehzelt, M.; Koch, N.; Heimel, G. Organic semiconductor density of states controls the energy level alignment at electrode interfaces. *Nature Communications* **2014**, *5*, 4174.

(51) Oehzelt, M.; Akaike, K.; Koch, N.; Heimel, G. Energy-level alignment at organic heterointerfaces. *Science Advances* **2015**, *1*, e1501127.

(52) Mendez, H.; Heimel, G.; Winkler, S.; Frisch, J.; Opitz, A.; Sauer, K.; Wegner, B.; Oehzelt, M.; Rothel, C.; Duhm, S.; Tobbens, D.; Koch, N.; Salzmann, I. Charge-transfer crystallites as molecular electrical dopants. *Nature Communications* **2015**, *6*, 8560.

(53) Hase, H.; Berteau-Rainville, M.; Charoughchi, S.; Bodlos, W.; Orgiu, E.; Salzmann, I. Critical dopant concentrations govern integer and fractional charge-transfer phases in doped P3HT. *Journal of Physics: Materials* **2022**, *6*, 014004.

(54) Aubry, T. J.; Winchell, K. J.; Salamat, C. Z.; Basile, V. M.; Lindemuth, J. R.; Stauber, J. M.; Axtell, J. C.; Kubena, R. M.; Phan, M. D.; Bird, M. J.; Spokoyny, A. M.; Tolbert, S. H.; Schwartz, B. J. Tunable Dopants with Intrinsic Counterion Separation Reveal the Effects of Electron Affinity on Dopant Intercalation and Free Carrier Production in Sequentially Doped Conjugated Polymer Films. *Adv. Funct. Mater.* **2020**, *30*, 2001800.

(55) Karpov, Y. et al. High Conductivity in Molecularly p-Doped Diketopyrrolopyrrole-Based Polymer: The Impact of a High Dopant Strength and Good Structural Order. *Adv. Mater.* **2016**, *28*, 6003–6010.

(56) Derewjanko, D.; Scheunemann, D.; Järsvall, E.; Hofmann, A. I.; Müller, C.; Kemerink, M. Delocalization Enhances Conductivity at High Doping Concentrations. *Advanced Functional Materials* **2022**, *32*, 2112262.

(57) Paterson, A. F.; Singh, S.; Fallon, K. J.; Hodsden, T.; Han, Y.; Schroeder, B. C.; Bronstein, H.; Heeney, M.; McCulloch, I.; Anthopoulos, T. D. Recent Progress in High-Mobility Organic Transistors: A Reality Check. *Adv. Mater.* **2018**, *30*, 0935–9648.

(58) Zeng, H.; Durand, P.; Guchait, S.; Herrmann, L.; Kiefer, C.; Leclerc, N.; Brinkmann, M. Optimizing chain alignment and preserving the pristine structure of single-ether based PBTTT helps improve thermoelectric properties in sequentially doped thin films. *J. Mater. Chem. C* **2022**, *10*, 15883–15896.

Graphical TOC Entry